Soft Matter

Cite this: *Soft Matter*, 2011, **7**, 4993

www.rsc.org/softmatter

PAPER

Microcontact printing for co-patterning cells and viruses for spatially controlled substrate-mediated gene delivery

Kellie I. McConnell,[a] John H. Slater,[a] Arum Han,[b] Jennifer L. West[a] and Junghae Suh*[a]

Received 26th October 2010, Accepted 15th March 2011
DOI: 10.1039/c0sm01209b

Spatial organization of gene expression is a crucial element in the development of complex native tissues, and the capacity to achieve spatially controlled gene expression profiles in a tissue engineering construct is still a considerable challenge. To give tissue engineers the ability to design specific, spatially organized gene expression profiles in an engineered construct, we have investigated the use of microcontact printing to pattern recombinant adeno-associated virus (AAV) vectors on a two dimensional surface as a first proof-of-concept study. AAV is a highly safe, versatile, stable, and easy-to-use gene delivery vector, making it an ideal choice for this application. We tested the suitability of four chemical surfaces (–CH_3, –COOH, –NH_2, and –OH) to mediate localized substrate-mediated gene delivery. First, polydimethylsiloxane stamps were used to create microscale patterns of various self-assembled monolayers on gold-coated glass substrates. Next, AAV particles carrying genes of interest and human fibronectin (HFN) were immobilized on the patterned substrates, creating a spatially organized arrangement of gene delivery vectors. Immunostaining studies reveal that –CH_3 and –NH_2 surfaces result in the most successful adsorption of both AAV and HFN. Lastly, HeLa cells were used to analyze viral transduction and spatial localization of gene expression. We find that –CH_3, –COOH, and –NH_2 surfaces support complete uniform cell coverage with high gene expression. Notably, we observe a synergistic effect between HFN and AAV for substrate-mediated gene delivery. Our flexible platform should allow for the specific patterning of various gene and shRNA cassettes, resulting in spatially defined gene expression profiles that may enable the generation of highly functional tissue.

Introduction

A significant hurdle in tissue engineering and regenerative medicine is the difficulty in achieving spatially organized tissue structures.[1] To drive the proper differentiation and assembly of cells, gene expression patterns may need to be tightly regulated. This may entail the expression of certain genes, involved in tissue genesis or repair, to be upregulated or downregulated in a spatially dependent manner. Among the advances in this field has been the incorporation of gene delivery agents, desired to guide the development of more native-like *in vitro* tissues. Pioneering methods of incorporating gene delivery in tissue engineering constructs involved the inclusion of plasmid DNA in polymeric matrices.[2] Since that time multiple groups have worked to create methods to deliver genetic material for tissue engineering applications, based on either the delivery of plasmid DNA or on viral transduction.[3–7]

Viral gene delivery is a promising alternative to the use of plasmid DNA for substrate-mediated gene delivery, also called reverse transfection or reverse transduction when non-viral or viral vectors are used, respectively. Viral particles can be easily modified to deliver a desired genetic cargo of either an over-expression or shRNA cassette. In recent years, several viruses have been used to control the delivery of genes for a variety of substrate-mediated applications, including targeted gene delivery for wound healing, bone remodeling, and prevention of restenosis.[8–10] Lentiviral and adenoviral vectors have been used to create cellular microarrays for upregulation or downregulation of genes of interest.[11–13] Pirone *et al.* implemented microcontact techniques for patterning adenovirus onto plastic.[5] Retroviruses have also been immobilized using alkanethiol self-assembled monolayers (SAMs), either through direct adsorption or through the use of a protein mediating layer.[4] Previous studies have shown that retrovirus is capable of interacting with extracellular matrix proteins, including fibronectin, to increase the gene delivery efficiency in target cell types.[14]

We set out to build upon these previous studies to advance the technology to the next level. First, we envisioned creating a platform where both viral gene delivery vectors and adhesive proteins can be co-patterned to control both cellular attachment and gene expression. This can ultimately enable us to modulate the virus pattern underneath the cell pattern, resulting in the creation of distinct regions of gene expression within the cell

[a]*Department of Bioengineering, Rice University, Houston, TX, 77030, USA. E-mail: jsuh@rice.edu*
[b]*Department of Electrical and Computer Engineering, Texas A&M University, College Station, TX, 77843, USA*

pattern. Furthermore, we desired to use a gene delivery vector that can be easily tailored to deliver genes into target cells with high efficiency. AAV is a relatively simple virus to modify, encoding only two viral genes: *rep* and *cap*. Modification of the *cap* gene can substantially improve the specificity and efficiency of AAV-mediated gene delivery. Numerous advances in AAV targeting have been made recently (reviewed by Schaffer *et al.*[15]), providing us with many potential options to enhance the selectivity of the vectors for specific cells. Eventually, by exploiting different combinations of virus patterns, cell patterns, transgenes, cell types, and AAV capsids (with different capsids targeting different cell types), we may be able to mimic the structure and function of highly complex tissues.

AAV is a small, 25 nm diameter replication deficient parvovirus that is being investigated intensively in 75 gene therapy clinical trials worldwide. AAV is considered to be one of the safest viral vectors for gene delivery, owing to several properties. First, approximately 80% of the human population is seropositive for this non-pathogenic virus, with no deleterious side effects.[16] AAV does not mediate insertional oncogenesis, which has been observed for retrovirus vectors,[17] and immunogenicity against the virus is substantially less than that of adenovirus vectors.[18] AAV is a non-enveloped virus composed of a protein shell encapsidating a 4.7 kb single stranded DNA genome. As mentioned above, the simple viral genome contains only two genes: *rep*, coding for non-structural replication proteins, and *cap*, coding for three proteins that self-assemble to form the viral capsid and a fourth protein that aids in this assembly.[19] A number of naturally occurring serotypes with diverse tropism and transduction profiles have been isolated.[20] The most commonly used serotype is AAV2, known to bind negatively charged heparin.[21] The crystal structure of this well-studied virus has been resolved.[22] In addition to the various serotypes, there are a variety of methods to alter the tropism of the virus in order to increase the gene delivery efficiency in a target cell population. These methods range from rationally inserting a targeting moiety into the capsid to using directed evolution to isolate an improved mutant out of a large pool of variants.[23–26] Lastly, AAV can be altered to deliver various genetic cargos, including overexpression cassettes as well as shRNA.[27,28] Collectively, the use of AAV for gene delivery in tissue engineering/regenerative medicine applications is a highly attractive choice due to its higher safety profile and ease of manipulation compared to other viral gene delivery systems, and the numerous methods to achieve target cell specificity and efficiency.

To spatially localize AAV2 vectors and cellular adhesion, we used microcontact printing of alkanethiols to create patterned self-assembled monolayers (SAMs). Microcontact printing techniques use elastomeric stamps with micron scale features to print molecules onto a surface.[29] For this work, we stamped alkanethiol chains onto gold-coated glass coverslips. Alkanethiol molecules are long carbon chains, with a functional group on one end and a gold binding sulfur molecule on the other end. Through van der Waals forces, the chains self-assemble into a monolayer of 2–3 nm in height at a 30° angle.[29] These SAMs form patterned features and can have either protein adhesive or protein resistive properties. Through this method, we are able to directly control the spatial localization of the virus, as opposed to adding it in a bulk solution and exposing all cells to the same gene delivery agent. In this work, we patterned chemistries that are potentially adhesive to both AAV2 and cellular attachment proteins.

We have developed a patterning platform to combine both the patterning of cells as well as AAV2 for gene delivery. Microcontact printing and a variety of alkanethiol surface chemistries have been used to identify a SAM that allows for both the attachment of cell adhesive proteins (human fibronectin, HFN) and reversible immobilization of AAV2. Relative attachment of both fibronectin and AAV2 was visualized and quantified using immunostaining. To test cell adhesion and the efficiency of viral transduction in this system, we used a green fluorescent protein (GFP) reporter gene and HeLa cervical cancer cells, which are known to be highly permissive to AAV2 transduction.[30] At various times post-cell seeding patterns were analyzed for both cellular attachment as well as efficiency of gene delivery.

Results and discussion

$-CH_3$ and $-NH_2$ surfaces most efficiently immobilize HFN

The ability to spatially control cell attachment to surfaces is an integral component in the creation of patterned cell constructs. We implemented microcontact printing to create 500 μm diameter circular patterns of one alkanethiol SAM, either a $-CH_3$, –COOH, $-NH_2$, or –OH terminated alkanethiol, surrounded by a biologically inert oligo(ethylene glycol) (–OEG) terminated SAM. Due to the passive nature of the –OEG SAM, HFN preferentially adsorbs to the circular patterns leaving the surrounding background free of protein. Using these alkanethiol molecules, we are able to create hydrophobic ($-CH_3$), hydrophilic (–OH), negatively charged (–COOH), and positively charged ($-NH_2$) surfaces. To study the efficacy of each surface chemistry ($-CH_3$, –COOH, $-NH_2$, and –OH) to mediate HFN binding and hence cell attachment, we used immunostaining and fluorescence microscopy to compare the amount of HFN that adsorbs to each SAM. The patterned surfaces were exposed to HFN, fluorescently immunolabeled, imaged under identical conditions, and the fluorescence integrated density of the patterned regions was measured. The hydrophobic $-CH_3$ SAM adsorbs the highest amount of HFN, displays uniform surface coverage (Fig. 1a and e) and was, therefore, used to normalize the integrated density values of the remaining surfaces. The $-NH_2$ patterned SAM shows a similar level of high and uniform attachment (Fig. 1c). The –COOH SAM results in immobilization of less HFN, 47% as compared to the $-CH_3$ SAM, and the patterns contain noticeable defects resulting in non-uniform HFN coverage (Fig. 1b and e). In these –COOH images, it is interesting to note that the defects appear as though the protein layer is peeling away. We believe that this happens because of the ten washing steps involved with immunostaining and they are seen in additional immunostaining images (Fig. 3b). In the later studies where cells are seeded on the surfaces, we do not perform these washing steps. The –OH pattern shows minimal HFN attachment and adsorbs only 23% of the HFN compared to the $-CH_3$ SAM (Fig. 1d and e). Previous studies that used non-patterned alkanethiol SAMs with varying functional groups showed similar results in protein adsorption and observed both surface wettability- and charge-dependent protein adsorption

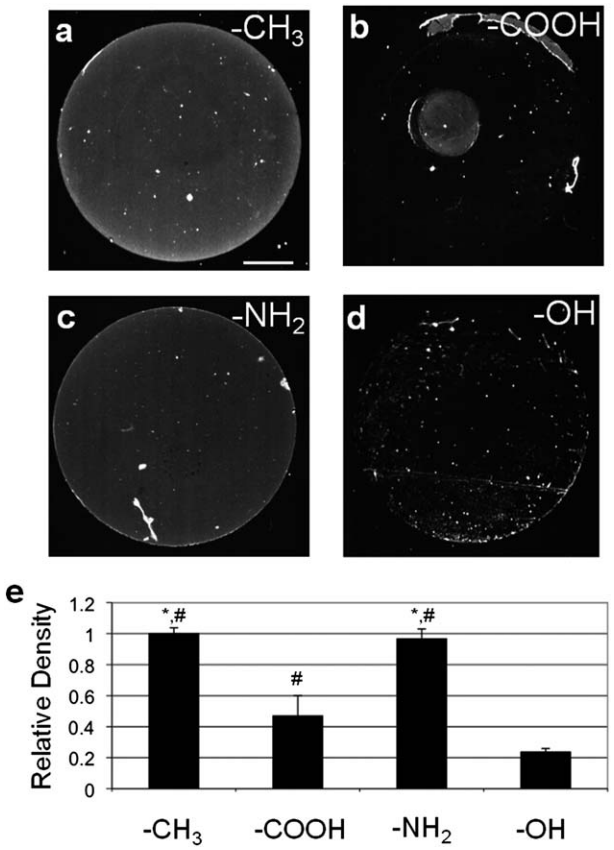

Fig. 1 Adsorption of HFN to micropatterned SAMs with varying functional groups. $–CH_3$ (a), –COOH (b), $–NH_2$ (c), and –OH (d) terminated alkanethiol SAMs were microcontact printed in 500 μm diameter circles, backfilled with an –OEG terminated SAM, exposed to HFN, fluorescently immunostained, imaged, and the integrated density of the patterns measured (e). The $–CH_3$ and $–NH_2$ terminated alkanethiol patterns (a and c) show a similar amount of adsorbed HFN. The –COOH (b) and –OH (d) surfaces show significantly less adsorption. Scale bar is 100 μm. (e) Relative amounts of HFN adsorbed to the various SAMs were determined by comparing the integrated densities (as quantified with ImageJ) of the circular patterns. Values were normalized to those of the $–CH_3$ spots. Error bars indicate standard error of the mean. The statistical significance ($p < 0.05$) is indicated with * for comparison against –COOH and # against –OH.

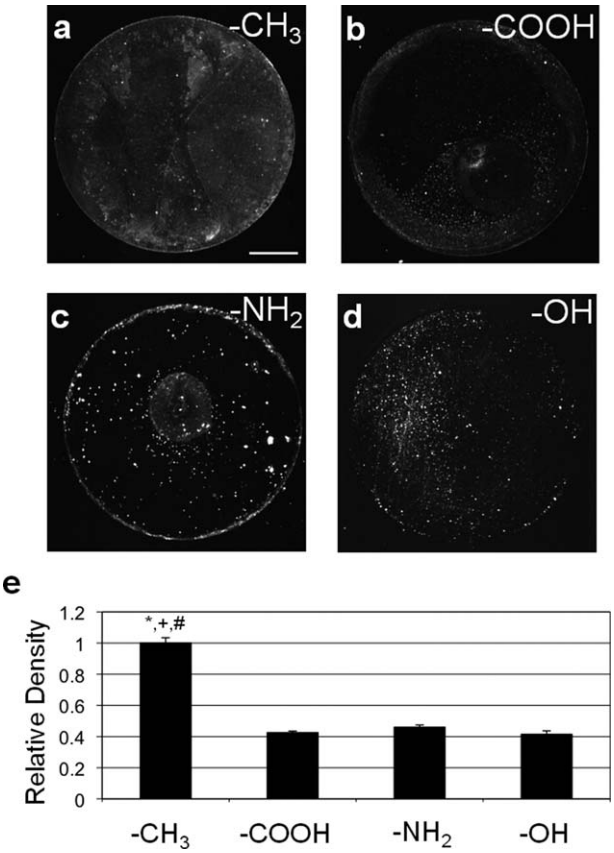

Fig. 2 Adsorption of AAV2 to micropatterned SAMs with varying functional groups. $–CH_3$ (a), –COOH (b), $–NH_2$ (c), and –OH (d) terminated alkanethiol SAMs were microcontact printed in 500 μm diameter circles, backfilled with an –OEG terminated SAM, exposed to AAV2, fluorescently immunolabeled, imaged, and the integrated density of the patterns measured (e). The $–CH_3$ terminated alkanethiol patterns (a) adsorb more AAV2 than –COOH (b), $–NH_2$ (c) or –OH (d) terminated alkanethiols. Scale bar is 100 μm. (e) Relative amounts of AAV2 adsorbed to the various SAMs were determined by comparing the integrated densities (as quantified with ImageJ) of the circular patterns. Values were normalized to those of the $–CH_3$ spots. Error bars indicate standard error of the mean. The statistical significance ($p < 0.05$) is indicated with * for comparison against –COOH, + against $–NH_2$, and # against –OH.

behavior.[31] The finding that HFN adsorbs to all of the SAMs tested indicates the potential of each SAM to support cell attachment. However, SAM-dependent differences in the amount of HFN adsorbed and in the uniformity of coverage could lead to differences in initial cell attachment, cellular proliferation, AAV2 adsorption, AAV2 transduction, and ultimately gene expression.

$–CH_3$ surfaces most efficiently immobilize AAV2

Similar to how spatial control of HFN adsorption is important for effective cell patterning, spatial control of AAV2 vector adsorption is crucial in spatial regulation of gene expression. To determine the efficacy of the four previously tested surfaces on AAV2 attachment, we repeated the adsorption analysis procedure used to quantify HFN adsorption. Micropatterned surfaces of the various functional group SAMs were exposed to AAV2, fluorescently immunolabeled, imaged under identical conditions, and the integrated densities measured. The various alkanethiol terminal groups yield different AAV2 immobilization patterns as well as variable amounts of virus attachment (Fig. 2). As with HFN attachment, the $–CH_3$ surface results in the highest adsorption of AAV2 with the most uniform coverage (Fig. 2a and e). The patterned –COOH, $–NH_2$, and –OH SAMs result in heterogeneous, non-uniform, punctate AAV2 coverage (Fig. 2b–d) with each SAM immobilizing 43%, 46%, and 41% of the amount adsorbed to the $–CH_3$ SAM, respectively (Fig. 2e). Overall, it appears that HFN and AAV2 both have similarly high affinities for the hydrophobic $–CH_3$ patterned SAMs. Interestingly, the surface charge seems to have little influence here on AAV2 adsorption as the –COOH and $–NH_2$ have similar levels of attachment. Furthermore, the antibody used in the

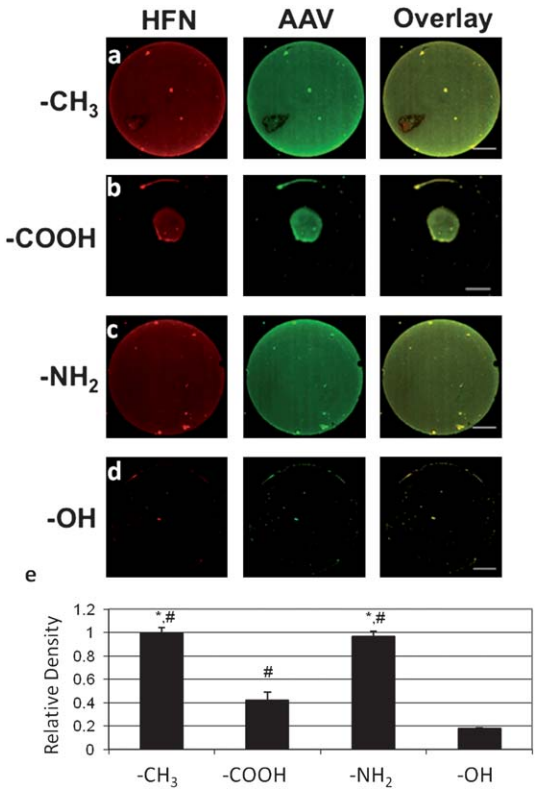

Fig. 3 Adsorption of AAV2 to pre-adsorbed HFN on micropatterned SAMs with varying functional groups. $-CH_3$ (a), –COOH (b), $-NH_2$ (c), and –OH (d) terminated alkanethiol SAMs were microcontact printed in 500 μm diameter circles, backfilled with an –OEG terminated SAM. Samples were pre-incubated with HFN and then exposed to AAV2, fluorescently immunolabeled, imaged, and the integrated density of the patterns measured (e). Images are pseudocolored for visualization of overlay. The left column shows HFN staining, the middle column shows AAV2 staining, and the right column is an overlay of the two channels. The $-CH_3$ and $-NH_2$ terminated pre-incubated patterns (a and c) adsorb more AAV2 than –COOH (b) or –OH (d) terminated alkanethiols. Scale bar is 100 μm. (e) Relative amounts of AAV2 adsorbed to the various SAMs were determined by comparing the integrated densities (as quantified with ImageJ) of the circular patterns. Values were normalized to those of the $-CH_3$ spots. Error bars indicate standard error of the mean. The statistical significance ($p < 0.05$) is indicated with * for comparison against –COOH and # against –OH.

immunostaining detects intact virus capsids only. Thus, the immobilized virus appears structurally intact and not denatured.

$-CH_3$ and $-NH_2$ surfaces most efficiently immobilize AAV2 and HFN

Patterned gene expression requires the attachment of both cell adhesive protein (HFN) and gene delivery vectors (AAV2) to the same micropatterned region. To achieve this, we patterned HFN and viral vectors together on one surface. For our studies, micropatterned SAM surfaces were exposed to HFN followed by incubation with AAV2. We rationalized that immobilizing HFN first will prevent this layer from sterically impeding the virus from gaining access to cells. The four different functional group SAMs were investigated and the samples were immunostained, imaged, and analyzed as described above. In this co-patterned case, the $-CH_3$ and $-NH_2$ (Fig. 3a and c) spots show qualitatively high, homogenous levels of attachment. Again, –COOH and –OH patterns display incomplete pattern coverage (Fig. 3b and d). As with Fig. 1b, we see a similar staining pattern for the –COOH surface that suggests washing away of the protein layer. The image shown in Fig. 3b is one example from the images taken, all of which showed a similar phenomenon. Quantitative measurements show that the $-CH_3$ and $-NH_2$ spots have statistically similar levels of AAV2 adsorption while the –COOH (42%) and –OH (18%) spots show significantly less (Fig. 3e). Since adsorption of both HFN and AAV is important for the viability of this technique, these qualitative and quantitative results for all surfaces suggest that AAV2 can successfully attach to a layer of HFN. In particular, homogenous coverage of AAV2 on the HFN pre-incubated $-CH_3$ and $-NH_2$ SAMs suggests that these surfaces will be particularly effective in supporting viral transduction, as seen previously with retrovirus.[4]

$-CH_3$, –COOH, and $-NH_2$ surfaces support cell adhesion and efficient gene delivery

The goal of this platform technology is to precisely pattern cells of interest and deliver desired genes *via* immobilized viral vectors. To determine the efficacy of both of these goals, we conducted cell studies using HeLa cells as a model. Cells were added to HFN and AAV2 co-patterned substrates to determine cell attachment and transduction. For the construct to be maximally successful, the pattern should be uniformly covered with cells and all cells should be expressing the virus encoded transgene, GFP. Alkanethiol patterns were incubated with HFN, then AAV2–GFP, and finally seeded with HeLa cells at a density of 100 cells per mm^2. Samples were imaged at 24, 48, and 72 h post-seeding and cell coverage and GFP expression were qualitatively observed. Minimal background cell attachment is seen in each case, indicating that the –OEG terminated alkanethiol surfaces provide an effective block to protein and cell attachment (Fig. 4). Three surfaces, $-CH_3$, –COOH, and $-NH_2$ (Fig. 4a–c), yield homogenous coverage of cells throughout the pattern. The –COOH surface may better retain the protein layer in this experiment, in comparison to immunostaining studies (Fig. 1 and 3), since we do not perform the ten washing steps when we seed cells. Cell attachment on the –OH patterned surface yields incomplete spot coverage (Fig. 4d). The viral vectors immobilized on the surfaces retain their infectivity, as seen by the robust GFP expression in the patterned cells for all four surfaces. This implies that vectors are able to efficiently release from the surfaces and are not denatured by immobilization.

At each time point, gene expression was quantified. Fluorescence for each time point was normalized to that of the $-CH_3$ samples at the 24 h time point. GFP expression increases over time for all four SAMs (Fig. 4e). At the 24 h time point, GFP expression is significantly higher for $-CH_3$ compared to the other 3 surfaces. All samples are similar at the 48 h time point. By the final 72 h time point, the –COOH spots have significantly higher overall GFP expression only when compared to the –OH surface. The –OH surface has a lower cell density compared to the other surfaces (73% average cell coverage). If the $-CH_3$ normalized integrated density at 72 h is adjusted to match the cell density of

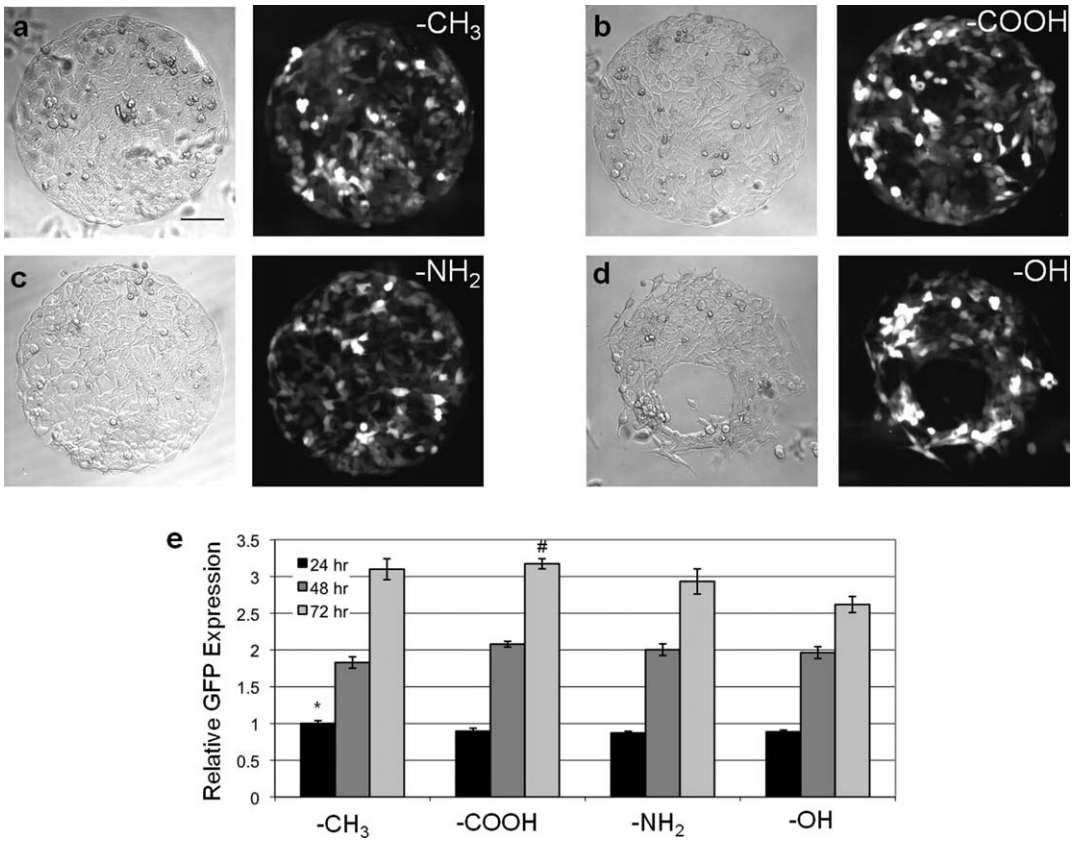

Fig. 4 Attachment and transduction of HeLa cells. Gold coated coverslips were patterned with –CH_3, –COOH, –NH_2, or –OH terminated alkanethiols in a spot pattern (a–d). Patterns were pre-incubated with HFN and then exposed to AAV2. Samples were rinsed and seeded with HeLa cells at a density of 100 cells per mm^2. Cells were imaged under DIC conditions to evaluate cell deposition (left image) and fluorescence to evaluate GFP expression (right image). Images shown are at 72 h time point. Scale bar is 100 μm. The fluorescence intensity was measured at 24, 48, and 72 h post-cell seeding (e). Values were normalized to the –CH_3 spot intensity at 24 h. Error bars indicate standard error of the mean. At 24 h, –CH_3 is significantly higher (*) than the other three surfaces ($p < 0.05$). At 48 h, all surfaces are similar. At 72 h, the statistical significance ($p < 0.05$) is indicated with # for comparison against –OH.

the –OH surface, the density will drop to 2.3—a value lower than the –OH integrated density of 2.6. This result suggests that cells on the –OH pattern have a slightly higher fluorescence per cell.

The ability to localize cells and deliver genes efficiently is a favorable outcome for this study. For three of the chemistries, pattern features are completely covered with cells, with almost no background or extension off the spots. As expected from immunostaining data, both the –CH_3 and –NH_2 surfaces support cell attachment and efficient gene delivery. However, the same cellular result is also true for the –COOH SAMs, a result that seems inconsistent with immunostaining data. From analyzing the images in Fig. 1b and 3b, we believe that the flaws in these patterns are due to the removal of protein during the successive wash steps in immunostaining. For cell studies, fewer washes are conducted, likely resulting in more protein remaining attached to the surface. Additionally, it is possible that even on surfaces adsorbing significantly less AAV (–COOH and –OH), there is still enough virus to transduce the overlying cells. If we assume that there is a complete monolayer of viral vectors on the HFN coated –CH_3 surfaces, this would equate to a multiplicity of infection (MOI) of 4×10^8 viral vectors per cell, based on the average cell density. Even with the lower amount of viral vectors seen on other surfaces, this would still lead to an MOI of 8×10^5 and 4×10^5 viruses per cell on the –COOH and –OH SAMs, respectively. These MOIs are substantially large and could lead to the high levels of expression observed on these surfaces. More quantitative analytical methods are currently under investigation to validate these hypotheses. Overall, gene expression is robust on all four SAMs, indicating that there are a variety of surface chemistries that can support this technique.

Cell transduction studies show high transduction of the patterned cell population. By transducing a large percentage of cells, we have the ability to efficiently modulate the behavior of the whole cell population. Ultimately, this process can be extended to the creation of more complex tissues using various cells, adhesive proteins, and gene delivery cassettes. Since cellular attachment and viral transduction are compatible with –CH_3, –NH_2, and –COOH surfaces, this may allow for the use of other adhesive proteins besides HFN. Other cell types may require different proteins for proper attachment and guidance, so this platform will be versatile for a number of systems. Additionally, AAV2 vectors are easily modifiable to include overexpression cassettes and shRNA cassettes, leading to the efficient upregulation and downregulation of many combinations of genes that may be of interest for tissue engineering applications. Moreover, AAV is an attractive viral platform because there are currently 12 identified serotypes, each serotype having the ability to deliver genetic cargo to different cell types within the body. The virus

can also be modified through the introduction of a targeting ligand into the virus capsid.[23,32] Finally, there are a number of directed evolution procedures that can be implemented to increase tropism to a desired cell type.[24–26,33–35] Overall, our versatile platform allows for the facile creation of different patterns, as well as the attachment and potential targeting of many cell types.

Interestingly, when AAV is adsorbed to an HFN layer, there are a variety of surface chemistries that are capable of supporting the surface immobilization needed for successful reverse transduction. Previous studies on retrovirus or adenovirus have suggested that virus adsorbed directly on $–CH_3$ terminated alkanethiol surfaces may denature or fail to release these viruses.[4,5] Similar to these results, we do not see acceptable transduction levels using AAV incubated directly onto SAMs. When analyzed on a $–CH_3$ SAM, we find that without the use of a mediating HFN layer, gene expression is only 13% of that seen with the HFN layer (Fig. 5a). Our immunostaining with an antibody that detects intact capsids only indicates the presence of undenatured AAV capsids on the $–CH_3$ surface (Fig. 2a). Therefore, inefficient release of AAV from the $–CH_3$ surface may be the more likely explanation for the poor reverse transduction. Most surfaces show an increase in virus attachment when HFN is present (Fig. 5b). HFN pre-adsorption on $–CH_3$ and –COOH SAMs yields an 80% increase in AAV2 attachment while pre-adsorption on $–NH_2$ surfaces yields an almost 300% increase. As seen with a previous retrovirus study, successful transduction is observed from $–CH_3$, –COOH, and $–NH_2$ surface chemistries when HFN is used as a protein mediating layer.[4] This was a surprising result given that retroviruses and AAV have substantial structural and functional differences between the two virus particle surfaces. Retroviruses are ~100 nm enveloped viruses, where the embedded envelope proteins mediate interactions of the virus with extracellular factors.[36] AAV, in contrast, are 25 nm non-enveloped viruses, where patches of amino acid residues displayed on capsid surfaces allow the virus to interact with extracellular factors.[21] These structural differences in conjunction with the knowledge that retroviruses and AAV infect different target cell types *in vivo*,[20,37] in part due to differences in virus particle surface–target cell surface interactions, we did not predict similar behavior of AAV and retroviruses on HFN. Further studies are necessary to determine more precisely how AAV is binding HFN.

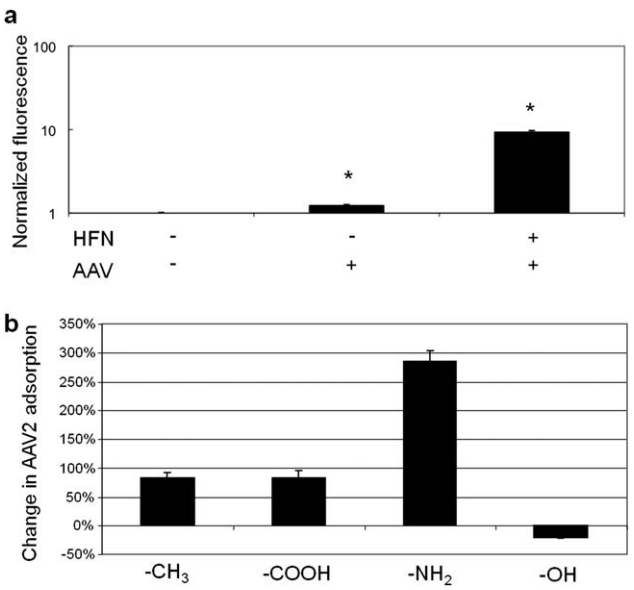

Fig. 5 AAV2 and HFN have a synergistic relationship. GFP expression was analyzed with or without the use of an HFN mediating layer on $–CH_3$ SAMs (a). When compared to autofluorescence of HeLa cells alone, fluorescence intensity measurements (as determined using ImageJ) are significantly higher ($p < 0.05$). However, AAV2 alone yields only 13% of the fluorescence measured in the HFN pre-incubated sample. To help explain this result, we compared the integrated density values from immunostaining AAV2 on SAMs alone *versus* AAV2 on HFN pre-incubated SAMs (b). When compared, HFN preincubation yields an 80% increase on $–CH_3$ and –COOH surfaces. For the $–NH_2$ surface, HFN pre-incubation yields an almost 300% increase in attachment. Pre-incubation leads to no improvement on the –OH SAM, instead causing a 20% decrease in attachment. Error bars represent standard error of the mean (a) and propagation of error (b).

An interesting outcome from this study was the discovery of a synergistic relationship between AAV2 and pre-adsorbed HFN. Specifically, the presence of HFN significantly improves the ability of AAV to reverse transduce cells. The quantity of virus that attaches to the substrate surface is higher when HFN is used to mediate adsorption. More interestingly, gene expression is nearly 8 times higher on surfaces pre-adsorbed with HFN. A possible explanation for this result is that AAV2 is able to bind HFN through electrostatic interactions. Previous reports have taken advantage of the negative charge of HFN in forming assembled layers.[38,39] AAV2 binds its natural receptor heparan sulfate, a negatively charged extracellular biomolecule, *via* patches of positively charged amino acids on the virus capsid.[21] It is possible that AAV2 is able to bind negatively charged HFN using a similar electrostatic mechanism. Different conformations of HFN exist when adsorbed on different surfaces, potentially exposing variable binding regions of the protein.[40,41] This variation in exposed HFN domains could yield changes in attachment and detachment of the virus to and from HFN that is adsorbed onto different chemistries. Previous reports have identified interactions between fibronectin and retrovirus,[14] suggesting binding to fibronectin may be a common feature between these two viruses. To our knowledge, no reports exist on AAV2 binding HFN, therefore, more in-depth quantitative investigations are necessary to support this potential explanation.

Microcontact printing is a versatile technique that has previously been applied to cellular localization studies.[42–44] Pattern formation for this method is simply controlled by the features on the elastomeric stamp and can easily be tailored to a desired size and pattern for a particular application. Additionally, various chemical surfaces can be created using different terminated alkanethiols. For this work we chose to test the efficacy of four different potentially protein adhesive groups: $–CH_3$, –COOH, $–NH_2$, and –OH. These various surfaces allowed us to test a spectrum of conditions, including hydrophobic/hydrophilic and negatively/positively charged surfaces, to determine the optimal conditions for HFN and virus attachment. It is imperative to create an efficient, reversible immobilization. To prevent protein from attaching to the non-patterned regions of the substrate, we utilized an oligo(ethylene glycol) terminated alkanethiol solution to create a protein resistant layer. This layer

successfully provided a crucial barrier to background protein attachment.

As tissue engineering strategies continue to develop, incorporation of gene delivery vectors presented in spatially meaningful ways may become increasingly important. Here, we have demonstrated the ability to spatially localize both cells and gene delivery vectors. Importantly, we overcame the concern of virus localization—viral vectors must be tightly localized, but also be able to release efficiently to transduce cells. By being able to control the deposition of extracellular matrix proteins and gene delivery vectors, we are able to control both cell localization and spatial gene delivery. In the future extension of this work, we will endeavor to create complex virus patterns underneath the cell patterns. This will lead to a clear advantage over creating cell patterns and adding gene vectors suspended in the bulk media. In this latter approach, all of the cells will be transduced by the viral vectors, yielding no formation of a gene expression pattern. In our approach, we should be able to pattern multiple different gene vectors, each encoding different transgenes, underneath a cell pattern. By combining variable virus patterns with cell patterns, complex blueprints for tissue genesis can be designed. Studies are underway to separate virus patterning from cell patterning so that these features can be controlled independently.

Experimental

Virus preparation

AAV2 was prepared as described previously.[45] Briefly, 293T cells and a triple transfection method were used to produce recombinant AAV2–GFP (AAV2 capsid with a green fluorescent protein (GFP) cassette under the cytomegalovirus (CMV) promoter). Cells were lysed 72 h post-transfection and virus was purified using ultracentrifugation and an iodixanol step gradient. Virus used for these studies remained in a solution of 40% iodixanol. Viral genomic titers were determined using quantitative polymerase chain reaction (QPCR) with primers against the CMV promoter. Virus used in this study was determined to have a concentration of 6.5×10^{11} vector genomes per ml.

PDMS stamp and coverslip preparation

Polydimethylsiloxane (PDMS) stamps were prepared by cast molding PDMS from a mold master that was fabricated by a photolithography process. First, a photoresist (SU-8™, Microchem, Inc., Newton, MA) layer was spin-coated on a 3-inch silicon wafer (SQI, Inc., Santa Clara, CA) and selectively exposed to UV light to transfer stamp patterns on the photomask to the SU-8™ layer. It was then immersed in a photoresist developer (Thinner P, Microchem, Inc., Newton, MA) and rinsed with isopropyl alcohol (IPA). To facilitate the release of PDMS stamps from the master after the cast molding process, the mold master was vapor-coated with (tridecafluoro-1,1,2,2-tetrahydrooctyl) trichlorosilane (United Chemical Technologies, Inc., Bristol, PA) for 10 min and briefly rinsed with IPA. The stamps were replicated by pouring PDMS pre-polymer (10 : 1 mixture, Sylgard® 184, Dow Corning, Inc., Midland, MI) on the mold master, followed by degassing inside a vacuum connected desiccator for 15–20 min to remove air bubbles and to completely fill the micropatterns with the PDMS. The degassed PDMS device was placed inside a leveled 85 °C oven for 1 h for polymerization. The fully polymerized PDMS device was then peeled off from the mold master and used as a microcontact printing stamp.

PDMS stamps presenting 500 μm diameter circles with a 1.2 mm pitch were cleaned by sonication in 100% ethanol. 35 mm diameter gold-coated glass coverslips (100 Å gold over 20 Å titanium, Platypus, Madison WI) were cleaned in dilute TL1 solution (6 : 1 : 1 $H_2O : NH_4OH : H_2O_2$) for 1 min at 80 °C, rinsed twice in Millipore purified water (MPH_2O), and dried with ultrapure nitrogen (N_2).

Surface functionalization

Alkanethiol solutions were diluted to 2 mM in 100% ethanol. Stamps were inked with either a $–CH_3$ (1-hexadecanethiol), –COOH (16-mercaptohexadecanoic acid), $–NH_2$ (11-mercapto-1-undecanol), or –OH (11-amino-1-undecanethiol hydrochloride) terminated alkanethiol, all from Sigma Aldrich (St Louis, MO). Stamps were dried with N_2, placed on a gold coverslip for 20 s, and gently removed. After printing, coverslips were incubated with 2 mM oligo(ethylene glycol) (–OEG) terminated alkanethiol (HSC_{11}-EG_6, Prochimia, Poland) for 1 h. Samples were rinsed twice with 100% ethanol and dried with N_2.

Protein attachment

Functionalized coverslips were incubated with 1 ml human fibronectin (HFN, Sigma Aldrich) warmed to 37 °C at a concentration of 25 μg ml^{-1} in phosphate buffered saline (pH 7.0, PBS) for 20 min at room temperature and rinsed dropwise with PBS. To adsorb virus, functionalized coverslips were incubated with 0.75 ml AAV2–GFP at a concentration of 6.5×10^{11} vector genomes per ml in 40% iodixanol for 30 min at room temperature and rinsed dropwise with PBS.

Immunostaining

HFN and/or AAV2 functionalized samples were blocked with 1% BSA in PBS for 1 h followed by gentle dropwise rinsing with PBS. HFN patterns were incubated with sheep anti-FN primary antibody (Abcam, Cambridge, MA) at 0.01 μg ml^{-1} overnight at 4 °C, rinsed with PBS, and exposed to donkey anti-sheep AlexaFluor 633 (AF633) conjugated antibody (Invitrogen, Carlsbad CA) at 0.02 μg ml^{-1} for 1 h at room temperature. Samples were rinsed dropwise with PBS, sterile water, and allowed to air dry. AAV2 patterns were incubated with A20 antibody (mouse anti-AAV2 capsid, American Research Products, Belmont, MA) at a concentration of 0.25 μg ml^{-1} overnight at 4 °C, rinsed with PBS, and exposed to goat-anti-mouse AlexaFluor 532 (AF532) conjugated antibody (Invitrogen) at a concentration of 10 μg ml^{-1} for 1 h at room temperature. Samples were rinsed dropwise with PBS and sterile water and allowed to air dry.

Cell studies

HeLa cells were seeded on functionalized surfaces in 60 mm tissue culture dishes at a density of 100 cells per mm^2. Cells were cultured in Dulbecco's Modified Eagle Medium (Invitrogen), supplemented with 10% fetal bovine serum and 1% penicillin/streptomycin (Invitrogen). Cells were maintained at 37 °C with 5% CO_2.

Imaging and image analysis

Images were acquired using a Zeiss LSM 5 LIVE confocal microscope (Carl Zeiss, Munich, Germany). Images within a given sample set (*i.e.* AAV2 adsorption, HFN adsorption, cell fluorescence) were acquired under identical conditions. GFP images were obtained using a 489 nm excitation at 1.8% power and data were collected for 2 ms pixel dwell time with a bandpass filter between 500 and 525 nm. Virus immunostaining images were collected using a 532 nm excitation at 50% power and data were collected for 2 ms pixel dwell time using a bandpass filter between 550 and 600 nm. HFN immunostaining images were collected using a 635 nm laser at 20% power and data were collected for 2 ms using a longpass 650 nm filter. Confocal control experiments were done to ensure no crosstalk between channels. To quantitatively compare the ability of each SAM to adsorb HFN and AAV2, the integrated densities of 15 spots (5 spots from 3 different stamps) were measured with ImageJ (NIH, Bethesda MD). For transduction studies, 5 fluorescence and differential interference contrast (DIC) images were taken at each time point. Integrated densities of fluorescence images were taken and values were normalized to those of $-CH_3$ samples at the 24 h time point. Data are given as the mean and standard error of the mean. JMP 9 software was used to determine the statistical significance ($p < 0.05$) using ANOVA and Tukey's HSD for post-hoc pair comparisons.

Conclusion

We have demonstrated the ability to precisely localize the immobilization of both extracellular matrix proteins and viral gene delivery vectors. Patterns were isolated to the desired area without background attachment. Through the use of micro-contact printing, we have shown there are a variety of surface chemistries capable of immobilizing both HFN and AAV, and allowing for efficient viral transduction and gene expression. This effective approach has been shown for HeLa cells and a model reporter gene but can be translated to other cell types and multiple AAV vectors delivering either overexpression or shRNA cassettes. In the future, more complicated structures can be created by patterning different combinations of adhesive proteins and viral vectors. Approaches such as this should support the future generation of structurally and functionally complex tissues.

Acknowledgements

The authors would like to thank Jordan Miller for his help with preliminary experiments. PDMS stamps were fabricated by Jaewon Park. We thank Melissa McHale for her help in editing the manuscript and Hadley Wickham for his help on statistical analysis. This work was supported by an NSF Graduate Research Fellowship to KIM. The AAV constructs were obtained from the Gene Therapy Center Vector Core at the University of North Carolina at Chapel Hill.

References

1 D. E. Discher, D. J. Mooney and P. W. Zandstra, *Science*, 2009, **324**, 1673–1677.
2 L. D. Shea, E. Smiley, J. Bonadio and D. J. Mooney, *Nat. Biotechnol.*, 1999, **17**, 551–554.
3 T. Houchin-Ray, K. J. Whittlesey and L. D. Shea, *Mol. Ther.*, 2007, **15**, 705–712.
4 C. A. Gersbach, S. R. Coyer, J. M. Le Doux and A. J. Garcia, *Biomaterials*, 2007, **28**, 5121–5127.
5 D. M. Pirone, L. Qi, H. Colecraft and C. S. Chen, *Biomed. Microdevices*, 2008, 561–566.
6 C.-W. K. Jau-Ye Shiu, W.-T. Whang and P. Chen, *Lab Chip*, 2010, **10**, 556–558.
7 F. Yamauchi, K. Kato and H. Iwata, *Biochim. Biophys. Acta*, 2004, **1672**, 138–147.
8 L. A. Chandler, J. Doukas, A. M. Gonzalez, D. K. Hoganson, D. L. Gu, C. Ma, M. Nesbit, T. M. Crombleholme, M. Herlyn, B. A. Sosnowski and G. F. Pierce, *Mol. Ther.*, 2000, **2**, 153–160.
9 I. Fishbein, I. S. Alferiev, O. Nyanguile, R. Gaster, J. M. Vohs, G. S. Wong, H. Felderman, I. W. Chen, H. Choi, R. L. Wilensky and R. J. Levy, *Proc. Natl. Acad. Sci. U. S. A.*, 2006, **103**, 159–164.
10 H. Ito, M. Koefoed, P. Tiyapatanaputi, K. Gromov, J. J. Goater, J. Carmouche, X. Zhang, P. T. Rubery, J. Rabinowitz, R. J. Samulski, T. Nakamura, K. Soballe, R. J. O'Keefe, B. F. Boyce and E. M. Schwarz, *Nat. Med.*, 2005, **11**, 291–297.
11 S. N. Bailey, S. M. Ali, A. E. Carpenter, C. O. Higgins and D. M. Sabatini, *Nat. Methods*, 2006, **3**, 117–122.
12 A. Oehmig, A. Klotzbucher, M. Thomas, F. Weise, U. Hagner, R. Brundiers, D. Waldherr, A. Lingnau, A. Knappik, M. H. Kubbutat, T. O. Joos and H. Volkmer, *BMC Genomics*, 2008, **9**, 441.
13 S. D. Raut, P. Lei, R. M. Padmashali and S. T. Andreadis, *J. Controlled Release*, 2010, **144**, 213–220.
14 H. Hanenberg, X. L. Xiao, D. Dilloo, K. Hashino, I. Kato and D. A. Williams, *Nat. Med.*, 1996, **2**, 876–882.
15 D. V. Schaffer, J. T. Koerber and K. I. Lim, *Annu. Rev. Biomed. Eng.*, 2008, **10**, 169–194.
16 B. J. Carter, *Mol. Ther.*, 2004, **10**, 981–989.
17 V. Nair, *Curr. Opin. Mol. Ther.*, 2008, **10**, 431–438.
18 A. K. Zaiss and D. A. Muruve, *Curr. Gene Ther.*, 2005, **5**, 323–331.
19 F. Sonntag, K. Schmidt and J. A. Kleinschmidt, *Proc. Natl. Acad. Sci. U. S. A.*, 2010, **107**, 10220–10225.
20 Z. Wu, A. Asokan and R. J. Samulski, *Mol. Ther.*, 2006, **14**, 316–327.
21 S. R. Opie, K. H. Warrington, Jr, M. Agbandje-McKenna, S. Zolotukhin and N. Muzyczka, *J. Virol.*, 2003, **77**, 6995–7006.
22 Q. Xie, W. Bu, S. Bhatia, J. Hare, T. Somasundaram, A. Azzi and M. S. Chapman, *Proc. Natl. Acad. Sci. U. S. A.*, 2002, **99**, 10405–10410.
23 W. Shi and J. S. Bartlett, *Mol. Ther.*, 2003, **7**, 515–525.
24 N. Maheshri, J. T. Koerber, B. K. Kaspar and D. V. Schaffer, *Nat. Biotechnol.*, 2006, **24**, 198–204.
25 O. J. Muller, F. Kaul, M. D. Weitzman, R. Pasqualini, W. Arap, J. A. Kleinschmidt and M. Trepel, *Nat. Biotechnol.*, 2003, **21**, 1040–1046.
26 W. Li, A. Asokan, Z. Wu, T. Van Dyke, N. Diprimio, S. J. Johnson, L. Govindaswamy, M. Agbandje-McKenna, S. Leichtle, D. Eugene Redmond, Jr, T. J. McCown, K. B. Petermann, N. E. Sharpless and R. J. Samulski, *Mol. Ther.*, 2008, 1252–1260.
27 R. S. Tomar, H. Matta and P. M. Chaudhary, *Oncogene*, 2003, **22**, 5712–5715.
28 D. Grimm, K. Pandey and M. A. Kay, *Methods Enzymol.*, 2005, **392**, 381–405.
29 Y. N. Xia and G. M. Whitesides, *Angew. Chem., Int. Ed.*, 1998, **37**, 551–575.
30 H. Hamilton, J. Gomos, K. I. Berns and E. Falck-Pedersen, *J. Virol.*, 2004, **78**, 7874–7882.
31 B. G. Keselowsky, D. M. Collard and A. J. Garcia, *J. Biomed. Mater. Res.*, 2003, **66**, 247–259.
32 L. M. Work, S. A. Nicklin, N. J. Brain, K. L. Dishart, D. J. Von Seggern, M. Hallek, H. Buning and A. H. Baker, *Mol. Ther.*, 2004, **9**, 198–208.
33 L. Perabo, D. Goldnau, K. White, J. Endell, J. Boucas, S. Humme, L. M. Work, H. Janicki, M. Hallek, A. H. Baker and H. Buning, *J. Virol.*, 2006, **80**, 7265–7269.
34 D. Grimm, J. S. Lee, L. Wang, T. Desai, B. Akache, T. A. Storm and M. A. Kay, *J. Virol.*, 2008, **82**, 5887–5911.
35 J. T. Koerber, J. H. Jang and D. V. Schaffer, *Mol. Ther.*, 2008, **16**, 1703–1709.

36 W. S. Hu and V. K. Pathak, *Pharmacol. Rev.*, 2000, **52**, 493–511.
37 E. Verhoeyen and F. L. Cosset, *J. Gene Med.*, 2004, **6**, S83–S94.
38 A. P. Ngankam, G. Mao and P. R. Van Tassel, *Langmuir*, 2004, **20**, 3362–3370.
39 C. R. Wittmer, J. A. Phelps, W. M. Saltzman and P. R. Van Tassel, *Biomaterials*, 2007, **28**, 851–860.
40 M. A. Lan, C. A. Gersbach, K. E. Michael, B. G. Keselowsky and A. J. Garcia, *Biomaterials*, 2005, **26**, 4523–4531.
41 V. Vogel and G. Baneyx, *Annu. Rev. Biomed. Eng.*, 2003, **5**, 441–463.
42 L. E. Dike, C. S. Chen, M. Mrksich, J. Tien, G. M. Whitesides and D. E. Ingber, *In Vitro Cell. Dev. Biol.*, 1999, **35**, 441–448.
43 R. Singhvi, A. Kumar, G. P. Lopez, G. N. Stephanopoulos, D. I. Wang, G. M. Whitesides and D. E. Ingber, *Science*, 1994, **264**, 696–698.
44 C. S. Chen, M. Mrksich, S. Huang, G. M. Whitesides and D. E. Ingber, *Science*, 1997, **276**, 1425–1428.
45 X. Xiao, J. Li and R. J. Samulski, *J. Virol.*, 1998, **72**, 2224–2232.